J. Fluid Mech. (2012), *vol.* 712, *pp.* 552–578.
doi:10.1017/jfm.2012.438

Thermally driven migration of ice-stream shear margins

Christian Schoof†

Department of Earth and Ocean Sciences, University of British Columbia, 6339 Stores Road, Vancouver, BC, V6T 1Z4, Canada

(Received 9 April 2012; revised 29 June 2012; accepted 4 September 2012; first published online 8 October 2012)

Ice-stream shear margins are the lateral boundaries of narrow, fast-flowing bands of ice within an ice sheet. We develop a theory for the migration of shear margins over time driven by viscous dissipation of heat within the ice, focusing on widening of the ice stream. The location of the margin is modelled as a transition from a cold to a temperate ice-sheet bed, and simultaneously as the transition from no slip to free slip at the same location. The temperature field in the ice is affected by intense shear heating as well as by the migration velocity of the margin (i.e. by the widening rate of the ice stream); if migration is too fast, there is little time for the ice to warm up and the margin remains cold, causing the bed to freeze. This suppresses widening. Conversely, if the migration speed is too slow, the ice in the margin warms up, causing the bed on the far side of the cold–temperate transition to reach the melting point, and migration to speed up. Using a Wiener–Hopf method, we show that for a given far-field shear stress, geothermal heat flux, and ice geometry, there is a single migration velocity that balances the two effects and permits widening at a steady rate. This velocity increases with the far-field lateral shear stress imposed by the ice stream, which controls shear heating in the margin. Our results also indicate that (i) a region of temperate ice must form in the margin, and that (ii) lateral advection of ice may play a significant role in controlling migration speeds.

Key words: contact lines, ice sheets, solidification/melting

1. Introduction

Ice streams are relatively narrow bands of fast flow within a larger continental ice sheet. A typical ice stream might be a kilometre thick, tens of kilometres wide and hundreds of kilometres long, while ice sheets can measure thousands of kilometres across. Despite their limited size, ice streams play an important role in the mass budget of ice sheets. In Antarctica, ice streams are estimated to account for over 80 % of the ice discharged from the continent (Bamber, Vaughan & Joughin 2000). Understanding their dynamics is therefore crucial to predicting future ice sheet behaviour as well as interpreting the geological record of ice sheet evolution.

Fast flow can result from several mechanisms. Pronounced troughs in underlying bedrock can channelize flow by permitting a greater amount of vertical shear. Greater ice thicknesses in these troughs also helps to insulate the lower layers of ice, allowing them to become warmer and less viscous. In some cases, impurities in the ice can also contribute to lower ice viscosities, and crystal alignment within the ice can

† Email address for correspondence: cschoof@eos.ubc.ca

similarly facilitate rapid shearing. However, the most dramatic spatial variations in ice flow velocities are associated with sliding at the base of the ice, and we focus exclusively on this mechanism here. Rapid sliding at the base is typically associated with the bed reaching the melting point and the presence of liquid water below the ice. This facilitates slip at the ice–bed interface as well as mechanical failure in underlying sediments (Blankenship *et al.* 1987; Kamb 1991; Iverson, Hooyer & Baker 1998; Tulaczyk, Kamb & Engelhardt 2000*a*; Alley & Bindschadler 2001). Sliding can account for all of the surface velocity of some ice streams (Engelhardt & Kamb 1997), and allows much faster ice flow than vertical shearing alone.

Ice streams often have sharp boundaries, with abrupt transitions from rapid to slow ice flow over a few kilometres (Echelmeyer *et al.* 1994; Harrison, Echelmeyer & Larson 1998). These lateral boundaries are referred to as *shear margins*. There may be situations in which steep-sided bedrock walls confine an ice stream and prevent its margin from moving, but in general, margins can migrate over time. Direct observations as well as indirect geophysical evidence show that the width of ice streams can evolve significantly on centennial time scales (Jacobel *et al.* 1996; Joughin *et al.* 2002; Siegert *et al.* 2004; Hulbe & Fahnestock 2007), but the processes involved are poorly understood.

A change in ice-stream width can have significant consequences for ice discharge. Assume a power-law rheology for ice ('Glen's law', see Cuffey & Paterson 2010), which sets $\tau_{ij} = BD^{1/n-1}D_{ij}$, where τ_{ij} is deviatoric stress, D_{ij} strain rate and D its second invariant. B and n are constants, with $n \approx 3$. Then discharge scales as ice-stream width to the power $(n + 2)$ provided the ice-stream flow is dominated by lateral shearing (Raymond 1996; van der Veen & Whillans 1996; Tulaczyk, Kamb & Engelhardt 2000*b*), as has been verified observationally for some ice streams on the Siple Coast of West Antarctica (Echelmeyer *et al.* 1994; Bindschadler *et al.* 1996; Joughin *et al.* 2002). Such a sensitive dependence of discharge on width indicates the need for a physics-based model for margin migration. However, no such model exists at present.

The sharp transition from slow to fast motion in ice-stream shear margins must correspond to an equally sharp transition in the properties of the ice sheet bed. High basal water pressure facilitates slip, and strong spatial variations in water pressure can therefore lead to an abrupt transition from rapid sliding where water pressure is high to slow or zero slip where water pressure is low. The models of ice-stream formation in Fowler & Johnson (1996) and Sayag & Tziperman (2008) are based on this notion. Alternatively, regions of high basal water pressure may be adjacent to parts of the bed that are frozen altogether. In fact, Fowler & Johnson's (1996) model predicts that the bed must freeze in some areas (see Díaz, Muñoz & Schiavi 2007). In that case, a shear margin can be expected to form at the transition between temperate and frozen parts of the bed, and this is the case we consider here.

The abrupt change from fast to slow flow generates large shear stresses and heating rates in the ice (Echelmeyer *et al.* 1994). Previous studies of shear margins (Raymond 1996; Jacobson & Raymond 1998; Schoof 2004) have focused on this effect, quantifying the effect of changes in the strength of the bed across the margin. Here, we aim to take this work further and develop a description of how the temperature response to shear heating controls margin migration. We focus exclusively on mechanisms that cause the ice stream to widen, so 'migration' here means movement of the margin into the slowly flowing ice surrounding the ice stream. We present a theory for the shrinkage of an ice stream in a separate paper (Schoof, in preparation).

Given the lack of observational constraints on the processes involved, we make a number of simplifying assumptions. These may need to be dispensed with in future; for now, our goal is to construct a minimal model that is capable of describing margin migration in a self-consistent way, in the expectation that this will help to identify the key processes involved. Our central assumption is that the margin corresponds to a transition from frozen to temperate bed, as well as from no slip to free slip. We will refer to the point at which this occurs as the 'transition point' throughout this paper. Similar mechanical assumptions have been made in Hutter & Olunloyo (1980) and Barcilon & MacAyeal (1993) for different geometries, and in Schoof (2004) for the shear margin geometry we will study below. As in those previous studies, we also restrict ourselves to a Newtonian rheology for ice, corresponding to $n = 1$ in Glen's law. A Newtonian rheology also requires a constant B in Glen's law, ignoring any temperature dependence of ice viscosity and hence any possible feedbacks between warmer ice and higher shearing rates.

Shear heating in the margin tends to warm the ice. By contrast, the effect of faster migration is to allow less time for the ice to warm up, as the margin is continually advancing into colder ice outside the ice stream. As a result, there exists a trade-off. If the margin were to migrate too rapidly, the ice would fail to warm up sufficiently. The bed on the temperate side of the transition point would start to freeze over, and further migration would be curtailed. On the other hand, if the margin were to migrate too slowly, heat would build up around the transition point and the temperature of the bed on the frozen side of the transition point would eventually reach the melting point. Migration would then need to speed up to keep pace with this warming of the bed. Steady migration velocities must therefore avoid both excessive accumulation of heat due to shear heating, and excessive cooling due to margin migration into colder ice. The theory we present in this paper shows that there is a single migration velocity that balances the two effects for a given shear heating rate.

The basic model for velocity and temperature is set out in § 2. We consider two constraints on the temperature field near the transition point between frozen and temperate bed (§ 3): the temperature on the frozen side of the transition point must remain below the melting point; and the bed on the temperate side of the transition point must not be in the process of freezing over. We show that these two constraints together determine a unique physically acceptable migration rate (§ 4). This rate depends on the magnitude of shear heating in the margins due to stresses imposed by the ice stream (§ 5). One of the implications of this result is that margin migration may be subject to a positive feedback, in which a widening of the ice stream leads to more shear heating in the margin and hence to faster widening (§ 6). Anticipating that this does not happen universally in ice streams, we also discuss some of the limitations and and necessary future extensions to the model in § 6.

Some of the material below is necessarily quite mathematical. The paper is arranged such that the more difficult material in §§4.2–4.3 can be omitted by readers interested primarily in the formulation of the model and the results rather than the details of the solution procedure.

2. Model

We consider the same geometry as in Schoof (2004), but focus on only one of the shear margins. That is, we model a parallel-sided inclined slab of ice of thickness H, with the x-axis oriented across the slab, and the y-axis pointing upwards perpendicularly to the slab (see figure 1). Assume that all dynamical quantities (such as ice velocity, pressure, temperature etc.) are independent of position in the downslope direction, and therefore depend only on (x, y). Consequently, the only non-

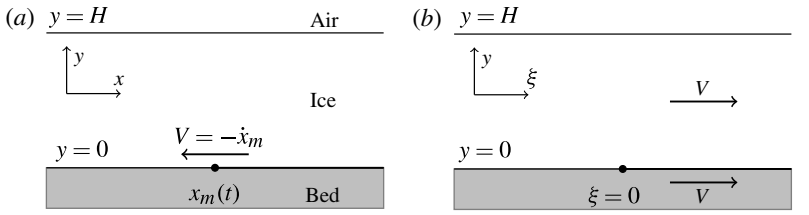

FIGURE 1. The geometry of the domain. Ice flow is into the page, with the ice ridge to the left and the ice stream to the right. Flow is driven by a lateral shear stress imposed from the right by the ice stream. The thick line at the bed indicates temperate (unfrozen) conditions, while the circle is the transition from frozen to temperate bed. In the stationary (x, y) frame shown in (a), the transition point $x_m(t)$ moves to the left at velocity V , while in the travelling wave frame with coordinates (ξ, y) shown in (b), the transition point is fixed at $(0, 0)$ but both ice and bedrock move transversely to the right at velocity V. This appears in the heat flow problem as an advection term, similar to the advection due to shearing flow in ice in Echelmeyer *et al.* (1994) and Jacobson & Raymond (1998).

zero velocity component is oriented in the downslope direction, and will be denoted by $u(x, y, t)$. Treating the ice as Newtonian with viscosity η, we model ice velocity as satisfying the appropriately reduced form of Stokes' equations,

$$\eta(u_{xx} + u_{yy}) = 0 \quad \text{for } 0 < y < H, \tag{2.1a}$$

$$\eta u_y = 0 \quad \text{on } y = H, \tag{2.1b}$$

$$\eta u_y = 0 \quad \text{on } y = 0,\ x > x_m(t), \tag{2.1c}$$

$$u = 0 \quad \text{on } y = 0,\ x < x_m(t), \tag{2.1d}$$

$$\eta u_x \to \begin{cases} \tau_s & \text{as } x \to +\infty, \\ 0 & \text{as } x \to -\infty, \end{cases} \tag{2.1e}$$

where subscripts denote partial derivatives.

Unlike in Schoof (2004), the model includes only one margin within the domain, assuming that the ice stream is much wider than the ice thickness. The bulk of the ice stream is represented by imposing a finite 'lateral' shear stress τ_s as a far-field boundary condition. This lateral shear stress scales as $\rho g W \sin\beta$, where β is the angle of inclination of the ice stream to the horizontal, and $W \gg H$ is ice-stream width. Hence τ_s is much larger than the typical driving stress $\rho g H \sin\beta$ generated in the margin itself, which is why we omit the gravitational body force in (2.1*a*).

Equations (2.1*c*) and (2.1*d*) correspond to an abrupt transition from no slip to the left of the transition point $x_m(t)$ to free slip on the right. We assume that this change in boundary conditions is associated with a switch in thermal conditions at the bed, so $x_m(t)$ is the position at which the bed goes from being temperate (at the melting point) to being frozen. In addition, we assume that friction on the temperate part of the bed is negligible. Again, this can be motivated by scaling considerations. In order for the bulk of the ice stream to be sliding rapidly, friction at the bed must be comparable to (or less than) the driving stress $\rho g H \sin\beta$. If friction in the shear margin remains comparable in magnitude to friction under the bulk of the ice stream, then it follows that this will be much smaller than the stress scale $\tau_s \sim \rho g W \sin\beta$ imposed by the bulk of the ice stream on the shear margin. Note that one might expect such comparable friction values if friction is controlled by pore pressure in subglacial sediment and if the bed under the shear margin is hydraulically well-connected to the ice stream,

so that pore pressures are therefore similar under the ice stream and under the shear margin.

In reality, one would probably not expect a perfect free slip to no slip transition; if the frozen ice–bed contact has a finite yield stress, then there will be at least a small zone of yielded bed on the frozen side, which could in principle be modelled using the method described in Schoof (2004). In keeping with our aim of a minimal model, we leave such additional processes for future research.

If the transition point $x_m(t)$ is the location at which the bed goes from temperate to frozen, then we must also model the temperature field $T(x, y, t)$. To simplify matters, assume that the ice stream and the underlying bedrock have the same thermal conductivity κ, and bulk heat capacity ρc, in the expectation that this will not make a qualitative difference to our results. Our geometry now leads to the following heat flow problem:

$$\rho c T_t - \kappa(T_{xx} + T_{yy}) = \eta(u_x^2 + u_y^2) \quad \text{for } 0 < y < H, \tag{2.2a}$$

$$\rho c T_t - \kappa(T_{xx} + T_{yy}) = 0 \quad \text{for } y < 0, \tag{2.2b}$$

$$T = T_s \quad \text{on } y = H, \tag{2.2c}$$

$$T^+ = T^- \quad \text{on } y = 0, \tag{2.2d}$$

$$-\kappa T_y^+ = -\kappa T_y^- \quad \text{on } y = 0,\ x < x_m(t), \tag{2.2e}$$

$$T = T_m \quad \text{on } y = 0,\ x > x_m(t), \tag{2.2f}$$

$$-\kappa T_y \sim q_{geo} \quad \text{as } y \to -\infty. \tag{2.2g}$$

In addition, lateral heat flux $-\kappa T_x$ must also vanish as $x \to \pm\infty$. Here, T_s is a constant surface temperature, T_m is the melting point of ice at the bed, and q_{geo} is an imposed geothermal heat flux. The superscripts $+$ and $-$ in (2.2*e*) indicate limits taken as the bed is approached from above and below, respectively. Physically, we have conductive heat flow in ice and bedrock, with heat generated by shear heating in the ice only. The temperature at the ice surface is fixed, while at the bed, different boundary conditions apply on the frozen and temperate sides of the transition point. On the frozen side, temperature and heat flux are both continuous but otherwise unspecified. On the temperate side, temperature is at the melting point. An important simplification that arises from our geometrical assumptions is that there is no advection of heat in (2.2*a*). In real ice-stream shear margins, there tends to be lateral inflow of ice that will lead to non-zero advective heat flux. We will discuss the implications of ignoring this flux in § 6.

Below, we assume that the time scale on which the temperature field in the margin adjusts can be treated as short compared with the time scale over which the lateral shear stress τ_s changes. This allows us to look for travelling wave solutions to (2.1)–(2.2). In doing so, we assume that the temperature field in the ice retains the same form relative to the moving transition point, at least on the time scale in question.

Define a travelling wave coordinate

$$\xi = x + Vt, \tag{2.3}$$

so that V is the velocity at which the margin migrates outward from the ice stream into the frozen bed. In this paper, we consider only the case $V > 0$, corresponding to a widening ice stream. The case of inward migration is dealt with in a separate paper. The main difference is that inward migration potentially requires a finite amount of water contained in the bed to freeze (see also appendix B), whereas here we allow sliding to commence as soon as the melting point is reached. That is, we assume that

only a very small amount of melting may be required to start sliding but a much larger amount of freezing may potentially be required to stop sliding.

Assume that u and T depend on x and t only through ξ, and that $x_m(t) = -Vt$. Then $\xi = 0$ represents the temperate–frozen transition in the moving coordinate frame. Our aim then becomes to identify how the margin migration velocity depends on the forcing parameters such as τ_s, q_{geo}, $T_m - T_s$ and H.

Equation (2.1) remains unchanged under this coordinate change, except that derivatives with respect to x are replaced with ξ-derivatives, and that $x < x_m$ becomes $\xi < 0$. The same is true for (2.2), except that (2.2*a*) and (2.2*b*) become

$$\rho c V T_\xi - \kappa(T_{\xi\xi} + T_{yy}) = \eta(u_\xi^2 + u_y^2) \quad \text{for } 0 < y < H, \tag{2.4a}$$

$$\rho c V T_\xi - \kappa(T_{\xi\xi} + T_{yy}) = 0 \quad \text{for } y < 0. \tag{2.4b}$$

The model as posed above is in fact insufficient to determine V: it lacks two additional physical constraints. First, we have assumed that the no-slip condition (2.1*d*) corresponds to a frozen bed, and consequently we have to ensure the bed to the left of x_m is really frozen. An obvious constraint is therefore to impose $T < T_m$ on the frozen side ($\xi < 0$). In addition the ice-stream bed on the temperate side ($\xi > 0$) should not be in the process of freezing if the margin is migrating to the left (i.e. into the frozen bed, with $V > 0$). This should be the case at least close to the transition point; we expand on this further in the next section and appendix B, where we show that, if freezing occurs close to the transition point, then migration must be to the right (i.e. into the ice stream). To ensure migration to the left, we require a non-negative net heat flux into the bed immediately to the right of the transition point. If we continue to use superscripts $+$ and $-$ to denote limits taken as the ξ-axis is approached from above and below, we can express this condition mathematically as $\kappa(T_y(\xi, 0)^+ - T_y(\xi, 0)^-) \geqslant 0$ at least for small positive ξ to ensure migration to the left. This corresponds to either zero net heat flux into the bed, or active melting at the ice–bed interface. Any water that is produced must then either be stored in an unfrozen layer of sediment at the bed, or evacuated by a drainage system at the ice–bed interface; the assumption of free slip above is tantamount to saying that this storage and drainage of water happens without affecting the flow of the ice in the shear margin.

We will see next that, taken together, these constraints impose restrictions on the form of possible singularities in heat flux near $\xi = 0$. Subsequently, we see in § 4 that, for a given temperature difference $T_s - T_m$, geothermal heat flux q_{geo} and thickness H, these restrictions then determine a unique migration velocity V for sufficiently large shear stresses τ_s, and show how to compute this.

3. The near-transition-point region

Although we will later provide a closed-form solution to (2.1), it is instructive to look purely at the local behaviour of solutions near the transition point at the origin. Defining plane-polar coordinates through $\xi = r\cos(\theta)$, $y = r\sin(\theta)$, (2.1*a*), (2.1*c*) and (2.1*d*) become

$$\frac{1}{r}(ru_r)_r + \frac{1}{r^2}u_{\theta\theta} = 0, \quad u_\theta(r, 0) = 0, \quad u(r, \pi) = 0. \tag{3.1}$$

The viscous dissipation rate must remain locally integrable, which constrains how singular the velocity field can be. The leading-order solution is then

$$u(r, \theta) = a_0 r^{1/2}\cos(\theta/2) + O(r^{3/2}). \tag{3.2}$$

Note that this corresponds to a singular stress field near $r = 0$, where $|\nabla u| \sim a_0/(2r^{1/2})$, while the velocity u remains bounded. The strength of the singularity is dictated by a_0, and this cannot be determined from the local problem alone. Instead, the far-field flow must be solved for. We will return to this in § 4.

Next, consider the leading-order local form of (2.4) with (2.2*f*) and (2.2*e*). Over sufficiently short length scales, the advection terms in (2.4) can be neglected. Assuming that $a_0 \neq 0$ (which as we will see in § 4 is the case for (2.1)), we then have (letting $T_m = 0$ without loss of generality)

$$-\kappa\left[\frac{1}{r}(rT_r)_r + \frac{1}{r^2}T_{\theta\theta}\right] = \frac{\eta a_0^2}{4r} \quad \text{for } 0 < \theta < \pi, \tag{3.3a}$$

$$-\kappa\left[\frac{1}{r}(rT_r)_r + \frac{1}{r^2}T_{\theta\theta}\right] = 0 \quad \text{for } \pi < \theta < 2\pi, \tag{3.3b}$$

$$T = 0 \quad \text{on } \theta = 0, \tag{3.3c}$$

$$T^+ - T^- = 0 \quad \text{on } \theta = \pi, \tag{3.3d}$$

$$-\kappa T_\theta^+ + \kappa T_\theta^- = 0 \quad \text{on } \theta = \pi. \tag{3.3e}$$

Subject to heat fluxes remaining locally integrable at the bed, this has solution (see appendix A)

$$T = b_0 r^{1/2}\sin(\theta/2) + c_0 r\sin(\theta) + T_h(r,\theta) + O(r^{3/2}), \tag{3.4a}$$

$$T_h(r,\theta) := \begin{cases} -\dfrac{\eta a_0^2}{4\kappa}\left[r(1-\cos(\theta)) + \dfrac{1}{\pi}\left(r\theta\cos(\theta) + r\log(r)\sin(\theta)\right)\right] \\ \quad \text{for } 0 < \theta < \pi, \\ -\dfrac{\eta a_0^2}{4\kappa}\left[-2r\cos(\theta) + \dfrac{1}{\pi}\left(r\theta\cos(\theta) + r\log(r)\sin(\theta)\right)\right] \\ \quad \text{for } \pi < \theta < 2\pi. \end{cases} \tag{3.4b}$$

It is straightforward to verify that this solution satisfies (3.3). As before, the coefficients b_0 and c_0 cannot be determined from the local problem alone, and the far-field temperature must be solved for. This becomes essential in solving for migration velocity V in the next section.

The solution (3.4) shows that there are two competing effects in operation near the transition point (figure 2). The first is the effect of the switch in boundary conditions, where a boundary at constant temperature (the melting point) is immediately adjacent to a region across which fluxes are continuous. This geometry is essentially that of a 'cooling fin', i.e. a narrow plate of a fixed, elevated temperature inserted into a colder medium (Carslaw & Jaeger 1959). This geometry in general leads to a singular heat flux: with $b_0 \neq 0$, the temperature gradient behaves as $|\nabla T| \sim b_0/(2r^{1/2})$. As before, the singularity strength b_0 is determined by the far-field temperature field, and it is therefore possible for b_0 to vanish under very specific conditions. We return to this in § 4. Note also that b_0 and c_0 both describe the effect of the cooling-fin geometry on its own, and do not represent the effect of near-field shear heating. The strength of the latter is determined by a_0, and appears in the solution through the inhomogeneous term T_h.

This shear heating rate is the second effect at work here. Note that the rate of shear heating in (3.3*a*) is singular. However, the resulting inhomogeneous term T_h is clearly bounded, and in fact leads to a weaker heat flux singularity than the cooling fin, with $|\nabla T_h| = O(\log r)$. Therefore the cooling-fin effect is dominant provided $b_0 \neq 0$, in which case T_h only appears at higher order.

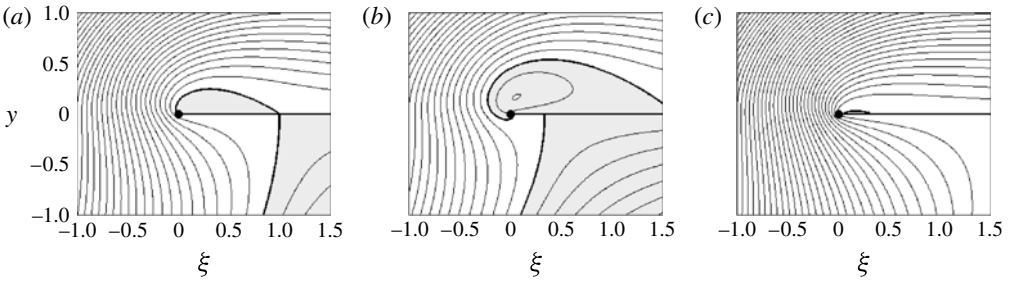

FIGURE 2. The solution (3.4) with $c_0 = 0$ and $\eta a_0^2/\kappa = 1$, ignoring the $O(r^{3/2})$ correction (which in general will be significant at sufficient distances from the origin, and change the shape of isotherms appreciably there), for: (*a*) $b_0 = 0$, (*b*) $b_0 = 0.4$, (*c*) $b_0 = -0.4$. Contour interval is 0.05, and $T > 0$ is shown shaded in grey; the $T = 0$ contour is a heavy black curve. The transition point is marked by a solid circle at the origin, and the boundary $y = 0$, $\xi > 0$ is shown as a heavy solid line. It is clear that the solution in (*b*) violates the stipulation that $T < 0$ at $y = 0$, $\xi < 0$. Hence the transition from slip to no slip cannot be located at $\xi = 0$ as assumed. Less obvious is that the bunched isotherms near the origin in (*c*) indicate a heat flux singularity that causes rapid heat loss from the temperate part of the bed, and hence freezing. The only viable local solution that can correspond to widening is (*a*).

To investigate the trade-off between these two effects further, assume for now that the cooling-fin geometry leads to a heat flux singularity, with $b_0 \neq 0$. We can then compute the temperature $T(r, \pi) \sim b_0 r^{1/2} - \eta a_0^2 r/(4\kappa) + O(r^{3/2})$ to the left of the transition point. We require that temperature at the bed for $\xi < 0$ ($\theta = \pi$) be negative: otherwise, the bed is not frozen locally, and we would not expect the no-slip boundary condition in (3.1) to hold. This leads to the conclusion that we must have $b_0 \leqslant 0$. However, we can also compute the net heat flux into the bed on the temperate side $\xi > 0$ of the transition point:

$$\kappa(T_\theta(r, 0) - T_\theta(r, 2\pi))/r \sim \kappa b_0 r^{-1/2} + O(r^{1/2}). \tag{3.5}$$

With $b_0 < 0$, this amounts to a negative heat flux into the bed; or in other words, to freezing of the bed.

In fact, the freezing rate is singular near the transition point, and this must result in the migration of the transition point to the right. A sketch of the relevant theory is given in appendix B; a more detailed treatment is given in a separate paper (Schoof, in preparation).

As our aim in the present paper is to study the widening of ice streams with $V > 0$, we are led to conclude that b_0 can neither be negative nor positive. Hence we must have $b_0 = 0$, and a logarithmic heat flux singularity at the origin (though heat flux into the temperate side of the bed at $\theta = 0$ remains bounded). Recall that b_0 is determined by the far-field behaviour of T, which in part depends on the migration velocity V. Below, we construct a Wiener–Hopf solution to the full problem consisting of (2.1) and (2.4) with (2.2*c*)–(2.2*g*) such that the local behaviour near the origin corresponds to $b_0 = 0$. As we will see, this constraint defines V implicitly as a function of the imposed forcing parameters, with V an increasing function of the applied lateral shear stress.

There is one major caveat to this procedure, however. If we set $b_0 = 0$, then the leading-order behaviour near the origin in the ice ($0 < \theta < \pi$) is given by

$$T(r, \theta) \sim -\frac{\eta a_0^2}{4\kappa} r \left[(1 - \cos(\theta)) + \frac{1}{\pi} (\theta \cos(\theta) + \log(r/r_0) \sin(\theta)) \right], \tag{3.6}$$

where $r_0 = \exp(4c_0\kappa/(\eta a_0^2))$. From this, it is straightforward to see that $T(r,\theta) > 0$ for small enough r and angles $\theta \in (0, \pi/2)$. Still ignoring higher-order terms (which may become important for finite $r \sim r_0$), the $T = 0$ isotherm is given by

$$r|_{T=0} = r_0 \exp\left(-\frac{\pi - (\pi-\theta)\cos(\theta)}{\sin(\theta)}\right), \tag{3.7}$$

and (3.6) predicts positive temperatures for $r < r|_{T=0}$. This is physically inconsistent as we expect $T \leqslant 0$ in the ice (ignoring for now any pressure-induced variations in melting point). This leads us to conclude that the actual local behaviour near the origin cannot in fact be described by (3.3) (or (2.4)) in a complete model: instead of a region of positive temperatures, there must be at least a small a region of 'temperate' ice. In the temperate ice, the temperature is then at the melting point, $T = 0$, and instead of pure ice, a partial melt with a non-zero fraction of liquid water must be present (e.g. Fowler 2001). Dissipation of heat in this region is then balanced by the production of further liquid, which can drain through connected veins between individual ice crystals driven by gravity and viscous compaction.

We ignore this complication in the remainder of the paper: implicitly, we are assuming that the formation of temperate ice does not significantly change the distribution of subtemperate ice (where $T < 0$) or the heat fluxes in the subtemperate ice. This allows us to develop a largely analytical approach below, but is unlikely to be valid. In effect, in regions where $T > 0$ in our model, T is then not an actual temperature variable but indicates a positive moisture content, and persisting with the heat equation (2.4) is tantamount to assuming that moisture transport in the temperate ice occurs down gradients of moisture content, and follows the same diffusive model as heat transport in subtemperate ice (such an 'enthalpy gradient' model was pioneered by e.g. Hutter, Yakowitz & Szidarowsky 1986; Aschwanden *et al.* 2012). However, this type of model is unlikely to be appropriate as there is no physical reason for flow to occur always down moisture content gradients (Fowler 2001), and future work will need to address the formation of temperate ice in greater detail.

4. Non-dimensionalization and solution

4.1. *The problem in scaled form*

First, we can reduce the number of free parameters in the model of § 2 by defining scales $[x] = H$, $[u] = \tau_s H/\eta$, $[T] = T_m - T_s$, $[V] = \kappa/(\rho c[x])$ and dimensionless variables through $(\xi, y) = [x](\xi^*, y^*)$, $u = [u]u^*$, $T = T_m + [T]T^*$, $V = [V]V^*$. This leaves two dimensionless parameters that measure the strength of geothermal heat flux and viscous dissipation,

$$\nu = \frac{q_{geo}[x]}{\kappa[T]}, \quad \alpha = \frac{\tau_s^2[x]^2}{\eta\kappa[T]}. \tag{4.1}$$

For simplicity, we immediately drop the asterisks on the dimensionless variables. The mechanical problem (2.1) then retains the same form, but with H, η and τ_s set to unity, with x replaced by ξ, and x_m set to zero. The scaled mechanical problem then contains no dimensionless parameters, and reads

$$u_{\xi\xi} + u_{yy} = 0 \quad \text{for } 0 < y < 1, \tag{4.2a}$$

$$u_y = 0 \quad \text{on } y = 1, \tag{4.2b}$$

$$u_y = 0 \quad \text{on } y = 0,\ \xi > 0, \tag{4.2c}$$

$$u = 0 \quad \text{on } y = 0,\ \xi < 0, \tag{4.2d}$$

$$u_\xi \to \begin{cases} 1 & \text{as } \xi \to +\infty, \\ 0 & \text{as } x \to -\infty. \end{cases} \tag{4.2e}$$

In dimensionless terms, the heat flow problem consisting of (2.2*c*)–(2.2*g*) and (2.4) becomes

$$VT_\xi - T_{\xi\xi} - T_{yy} = \alpha a \quad \text{for } y > 0, \tag{4.3a}$$

$$VT_\xi - T_{\xi\xi} - T_{yy} = 0 \quad \text{for } y < 0, \tag{4.3b}$$

$$T = -1 \quad \text{on } y = 1, \tag{4.3c}$$

$$T^+ = T^- \quad \text{on } y = 0, \tag{4.3d}$$

$$-T_y^+ = -T_y^- \quad \text{on } y = 0,\ \xi < 0, \tag{4.3e}$$

$$T = 0 \quad \text{on } y = 0,\ \xi > 0, \tag{4.3f}$$

$$T_y \to -\nu \quad \text{as } y \to -\infty, \tag{4.3g}$$

where

$$a := u_\xi^2 + u_y^2 \tag{4.4}$$

is independent of the dimensionless parameters in the problem. We see that α is a dimensionless measure of the strength of heating, while the spatial distribution of heating is always the same. From the definition of α, it is clear that its size is dictated by a trade-off between depth-integrated dissipation, which scales as $\tau_s^2[x]/\eta$, and a background heat flux driven by temperature differences between bed and surface, scaled as $\kappa[T]/[x]$. Note also that ν is simply the ratio of geothermal heat flux to that background heat flux, and is therefore a measure of the extent to which geothermal heat flux can supply that background heat loss from the bed; $1 - \nu$ is then a scaled measure of net rate of heat loss that the temperate part of the bed would experience in the absence of dissipation. We will later see that the dimensionless group $\alpha/(1 - \nu)$ is key in determining the scaled velocity V^*. This can be interpreted more straightforwardly as the ratio of depth-integrated heat dissipation to the net rate of cooling of the bed that would occur in the absence of dissipation.

The solution procedure in §§ 4.2–4.3 below – which the less mathematically inclined reader can skip – shows that the scaled migration rate V^* (or V in (4.3), as we have just omitted asterisks) is a function of the shear heating strength parameter α, which in turn is a scaled lateral shear stress τ_s from (4.1).

4.2. *Wiener–Hopf solution and the relationship between V and dimensionless shear heating strength α*

The mechanical problem (4.2) is easy to solve using the same method as in Schoof (2004). A closed-form solution can be found as

$$u_\xi - iu_y = \frac{\exp\left(\dfrac{\pi z}{2}\right)}{\left[\exp(\pi z) - 1\right]^{1/2}}, \tag{4.5}$$

where $z = \xi + \mathrm{i}y$ and the square root is the usual branch. It is easy to verify that (2.1*a*) is satisfied as a Cauchy–Riemann condition, and that (4.5) also satisfies all the boundary conditions in (2.1). The rate of heat production is therefore given in

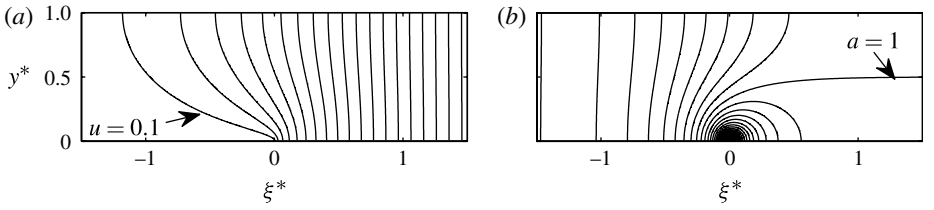

FIGURE 3. (*a*) Contours of $u(\xi, y)$ at contour intervals of 0.1. (*b*) The corresponding heating rate $a(\xi, y) = u_\xi^2 + u_y^2$, with the same contour intervals.

dimensionless form by (see figure 3)

$$a = \frac{\exp\left(\dfrac{\pi\xi}{2}\right)}{2\sqrt{\sinh^2\left(\dfrac{\pi\xi}{2}\right) + \sin^2\left(\dfrac{\pi y}{2}\right)}}. \tag{4.6}$$

This shows that the singularity strength in § 3 is given in dimensionless terms by $a_0^2 = 1/\pi$.

Next, we need to solve the thermal problem (4.3). Note that $a \to 1$ exponentially as $x \to +\infty$ from (4.6); a is therefore not integrable. To facilitate the use of Fourier transforms, define a reduced temperature Θ through

$$T(\xi, y) = \begin{cases} -1 + \nu(1-y) + \dfrac{\alpha}{2}\phi(\xi)y(1-y) + \Theta(\xi, y) & \text{for } 0 < y < 1, \\ -1 + \nu(1-y) + \Theta(\xi, y) & \text{for } y < 0, \end{cases} \tag{4.7}$$

where ϕ is a twice continuously differentiable cut-off function that satisfies $\phi(\xi) = 0$ for $\xi < \xi_1$ and $\phi(\xi) = 1$ for $\xi > \xi_2$, with $\xi_2 > \xi_1 > 0$ fixed; a possible choice for $\xi_1 \leqslant \xi \leqslant \xi_2$ is

$$\phi(\xi) = 3\zeta^5/16 - 5\zeta^3/8 + 15\zeta/16 + 1/2 \quad \text{where } \zeta := -1 + 2(\xi - \xi_1)/(\xi_2 - \xi_1). \tag{4.8}$$

This is a simple change of variable from T to Θ, and does not affect the uniqueness of solutions. In particular, for a given V, the governing equations (4.9) below are linear, and different choices of cut-off function ϕ, say ϕ_1 and ϕ_2, merely lead to different values of Θ related through $\Theta_2 = \Theta_1 + \alpha(\phi_1 - \phi_2)y(1-y)$ for $0 < y < 1$, and $\Theta_2 = \Theta_1$ for $y < 0$. V is determined ultimately by enforcing the behaviour of T, and hence Θ, to be $o(r^{1/2})$ near the origin. But ϕ_1 and ϕ_2 vanish near the origin, and hence Θ_1 and Θ_2 computed from (4.9) with the same V have the same local behaviour. Therefore, if a certain value of V generates the correct $o(r^{1/2})$ behaviour for one choice of ϕ, it also does so for the other, and the correct V cannot depend on the choice of cut-off function ϕ.

A similar complication to a being non-integrable is that the constant term on the right-hand side of (4.3*c*) is also not integrable. In common with similar problems in fluid dynamics (e.g. Barcilon & MacAyeal 1993), we regularize this term in order to apply the Wiener–Hopf method. Let the function $\Theta_\epsilon(\xi, y)$ satisfy the following regularized problem:

$$V\Theta_{\epsilon,\xi} - \Theta_{\epsilon,\xi\xi} - \Theta_{\epsilon,yy} = \alpha b \quad \text{for } y > 0, \tag{4.9a}$$

$$V\Theta_{\epsilon,\xi} - \Theta_{\epsilon,\xi\xi} - \Theta_{\epsilon,yy} = 0 \quad \text{for } y < 0, \tag{4.9b}$$

$$\Theta_\epsilon = 0 \qquad \text{on } y = 1, \tag{4.9c}$$

$$\Theta_\epsilon^+ = \Theta_\epsilon^- \qquad \text{on } y = 0, \tag{4.9d}$$

$$-\Theta_{\epsilon,y}^+ = -\Theta_{\epsilon,y}^- \qquad \text{on } y = 0,\ \xi < 0, \tag{4.9e}$$

$$\Theta_\epsilon = (1-\nu)\exp(-\epsilon\xi) \qquad \text{on } y = 0,\ \xi > 0, \tag{4.9f}$$

$$\Theta_{\epsilon,y} \to 0 \qquad \text{as } y \to -\infty. \tag{4.9g}$$

Here

$$b(\xi, y) := a(\xi, y) - \phi(\xi) - V\phi'(\xi)y(1-y)/2 + \phi''(\xi)y(1-y)/2 \tag{4.10}$$

as well as the exponential term on the right-hand side of (4.9*f*) are integrable. Θ satisfies (4.9), but with the right-hand side of (4.9*f*) replaced by $1-\nu$, which corresponds to the limit $\epsilon \to 0$. We proceed on the standard assumption that $\lim_{\epsilon\to 0}\Theta_\epsilon(\xi, y) = \Theta(\xi, y)$ pointwise in (ξ, y). That is, we find the solution to (4.9) for finite ϵ, and then take the limit $\epsilon \to 0$.

Define the Fourier transform of a function $f(\xi)$ as

$$\mathscr{F}(f)(k) = \hat{f}(k) := \int_{-\infty}^{\infty} f(\xi)\exp(-\mathrm{i}k\xi)\,\mathrm{d}\xi. \tag{4.11}$$

Then $\hat{\Theta}_\epsilon$ satisfies

$$-\hat{\Theta}_{\epsilon,yy} + (k^2 + \mathrm{i}Vk)\hat{\Theta}_\epsilon = \alpha\hat{b} \qquad \text{for } y > 0 \tag{4.12a}$$

$$-\hat{\Theta}_{\epsilon,yy} + (k^2 + \mathrm{i}Vk)\hat{\Theta}_\epsilon = 0 \qquad \text{for } y < 0. \tag{4.12b}$$

Using the method of variation of coefficients, a solution that satisfies the surface and far-field boundary conditions (4.9*c*) and (4.9*g*) takes the form

$$\hat{\Theta}_\epsilon(k, y) = \alpha\left[\int_y^1 \frac{\sinh[m(1-y')]}{m\sinh(m)}\hat{b}(k, y')\,\mathrm{d}y'\right]\sinh(my) + \alpha\left[\int_0^y \frac{\sinh(my')}{m\sinh(m)}\hat{b}(k, y')\,\mathrm{d}y'\right]\sinh[m(1-y)] + A\sinh[m(1-y)] \tag{4.13a}$$

for $0 < y < 1$, and

$$\hat{\Theta}_\epsilon(k, y) = B\exp(my) \tag{4.13b}$$

for $y < 0$, where

$$m = (k^2 + \mathrm{i}kV)^{1/2} \tag{4.14}$$

has branch cuts on the imaginary k-axis for $\mathrm{Im}(k) > 0$ and $\mathrm{Im}(k) < -V$, and behaves as $m \sim |k|$ for large real k. Continuity of Θ_ϵ at $y = 0$, equation (4.9*d*), further requires

$$A\sinh(m) = B. \tag{4.15}$$

Next, define

$$F(\xi) = \Theta_\epsilon(\xi, 0) - (1-\nu)\exp(-\epsilon|\xi|), \quad G(\xi) = \Theta_{\epsilon,y}^+(\xi, 0) - \Theta_{\epsilon,y}^-(\xi, 0). \tag{4.16}$$

Then $F(\xi) = 0$ for $\xi > 0$ and $G(\xi) = 0$ for $\xi < 0$, so that $\hat{F}(k) = \hat{F}^+(k)$ and $\hat{G}(k) = \hat{G}^-(k)$ are analytic in the upper and lower halves of the complex-k-plane, respectively (Noble 1958). (Note that references to plane geometry below all concern

the k-plane.) On the real axis, we then have

$$\hat{F}^+(k) = B - (1-\nu)\left(\frac{1}{\epsilon + \mathrm{i}k} + \frac{1}{\epsilon - \mathrm{i}k}\right) \tag{4.17}$$

from (4.9*f*), and

$$\hat{G}^-(k) = \alpha \int_0^1 \frac{\sinh[m(1-y)]}{\sinh(m)} \hat{b}(k, y)\,\mathrm{d}y - m\cosh(m)A - mB \tag{4.18}$$

from (4.9*e*). Eliminating A and B between (4.15), (4.17) and (4.18) finally leads to the standard Wiener–Hopf problem (Noble 1958)

$$\hat{G}^-(k) = W(k)\hat{F}^+(k) + h(k), \tag{4.19}$$

where

$$W(k) = -(k^2 + \mathrm{i}kV)^{1/2} \frac{\exp\left[(k^2 + \mathrm{i}kV)^{1/2}\right]}{\sinh\left[(k^2 + \mathrm{i}kV)^{1/2}\right]}, \tag{4.20}$$

$$\begin{aligned} h(k) = {} & (1-\nu)W(k)\left(\frac{1}{\epsilon + \mathrm{i}k} + \frac{1}{\epsilon - \mathrm{i}k}\right) \\ & + \alpha \int_0^1 \frac{\sinh\left[(k^2 + \mathrm{i}kV)^{1/2}(1-y)\right]}{\sinh\left[(k^2 + \mathrm{i}kV)^{1/2}\right]} \hat{b}(k, y)\,\mathrm{d}y. \end{aligned} \tag{4.21}$$

First, we need to construct a decomposition $W(k) = W^+(k)/W^-(k)$, where W^+ and W^- are continuous and non-zero on the real axis and can be continued analytically into the lower and upper half-planes, respectively. Let

$$W_2(k) = \frac{k^{1/2}\exp\left[(k^2 + \mathrm{i}kV)^{1/2}\right]}{2\,(k - \mathrm{i}V)^{1/2}\sinh\left[(k^2 + \mathrm{i}kV)^{1/2}\right]}, \tag{4.22}$$

where $k^{1/2}$ and $(k - \mathrm{i}V)^{1/2}$ behave as the principal value of $\sqrt{k}$ when $k \to +\infty$ along the real axis, and have branch cuts on the positive half of the imaginary axis, extending upwards from branch points at the origin and at $k = \mathrm{i}V$ respectively. Meanwhile, $(k^2 + \mathrm{i}kV)^{1/2} = m$ is the same branch as before. Then $W_2(k)$ is Hölder continuous and non-zero on the real axis, and behaves as $W_2(k) \sim 1 + \mathrm{i}V/2k$ for large real $k \to \pm\infty$. In fact, $W_2(k)$ never crosses the negative real axis for real k, so $\log(W_2(k))$ is Hölder continuous if the usual branch of the logarithm is used.

A standard decomposition using Plemelj's formulae can therefore be written as $W_2(k) = W_2^+(k)/W_2^-(k)$, where

$$W_2^\pm(k) = \exp\left(\frac{1}{2\pi\mathrm{i}}\int_{-\infty}^{\infty} \frac{\log(W_2(k'))\,\mathrm{d}k'}{k - k'}\right), \tag{4.23}$$

choosing superscripts $+$ and $-$ for k in the upper and lower half-planes, respectively.

We have $W(k) = -2\,(k + \mathrm{i}V)^{1/2}\,(k - \mathrm{i}V)^{1/2}\,W_2(k)$, where $(k + \mathrm{i}V)^{1/2}$ has a branch cut extending from $k = -\mathrm{i}V$ downwards along the negative imaginary axis, and again behaves as the principal value of $\sqrt{k}$ when $k \to +\infty$. The appropriate factorization is

therefore (Noble 1958, see in particular exercise 1.12)

$$W^+(k) = -2\,(k + \mathrm{i}V)^{1/2}\,W_2^+(k), \quad W^-(k) = \frac{W_2^-(k)}{(k - \mathrm{i}V)^{1/2}}. \tag{4.24}$$

For $k \to \infty$ in the upper and lower half-planes, we have $W_2^{\pm}(k) \to 1$ by construction; in fact, with $W_2(k) \sim 1 + \mathrm{i}V/2k$ for large k, we expect $W_2^{\pm}(k) \sim 1 + \mathrm{i}V\log(k)/(4\pi k) + O(1/k)$. It follows that $W^+(k) \sim k^{1/2}/2$ and $W^-(k) \sim k^{-1/2}$. This behaviour will be key later in determining the limiting behaviour of heat flux $G(\xi)$ at the origin, which we have already constrained in § 3. We will then use this limiting behaviour to derive a constraint on migration velocity V.

The standard Wiener–Hopf method now re-writes (4.19) as $W^-(k)\hat{G}^-(k) = W^+(k)\hat{F}^+(k) + W^-(k)h(k)$, and decomposes the inhomogeneous term additively into functions f^+ and f^- that can be continued analytically into the upper and lower half-planes, i.e. $W^-(k)h(k) = f^+(k) - f^-(k)$. Then

$$W^-(k)\hat{G}^-(k) + f^-(k) = W^+(k)\hat{F}^+(k) + f^+(k), \tag{4.25}$$

so that the left- and right-hand sides are analytic continuations of one another, and are therefore representations of the same entire function $\Omega(k)$ in the lower and upper half-planes. Once that function has been found, $\hat{G}^+$ and $\hat{F}^-$ are fully determined.

The next step is to find f^- and f^+. We have

$$\begin{aligned} W^-(k)h(k) = (1-\nu)W^+(k)&\left(\frac{1}{\epsilon + \mathrm{i}k} + \frac{1}{\epsilon - \mathrm{i}k}\right) \\ &+ \alpha W^-(k)\int_0^1 \frac{\sinh\left[(k^2 + \mathrm{i}kV)^{1/2}(1-y)\right]}{\sinh\left[(k^2 + \mathrm{i}kV)^{1/2}\right]}\hat{b}(k,y)\,\mathrm{d}y. \end{aligned} \tag{4.26}$$

Trivially, $W^+(k)/(\epsilon - \mathrm{i}k)$ can be continued analytically into the upper half-plane. To decompose the remainder of W^-h, we can use Plemelj's formulae. For k in the lower half-plane, we get

$$\begin{aligned} f^-(k) &= \frac{1-\nu}{2\pi\mathrm{i}}\int_{-\infty}^{\infty}\frac{W^+(k')\,\mathrm{d}k'}{(\epsilon + \mathrm{i}k')(k' - k)} \\ &\quad + \frac{\alpha}{2\pi\mathrm{i}}\int_{-\infty}^{\infty}\frac{W^-(k')}{k' - k}\left[\int_0^1 \frac{\sinh\left[(k'^2 + \mathrm{i}k'V)^{1/2}(1-y)\right]}{\sinh\left[(k'^2 + \mathrm{i}k'V)^{1/2}\right]}\hat{b}(k',y)\,\mathrm{d}y\right]\mathrm{d}k' \\ &= -\frac{(1-\nu)W^+(\mathrm{i}\epsilon)}{\epsilon + \mathrm{i}k} + \frac{\alpha}{2\pi\mathrm{i}}\int_{-\infty}^{\infty}\frac{W^-(k')}{k' - k} \\ &\quad \times \left[\int_0^1 \frac{\sinh\left[(k'^2 + \mathrm{i}k'V)^{1/2}(1-y)\right]}{\sinh\left[(k'^2 + \mathrm{i}k'V)^{1/2}\right]}\hat{b}(k',y)\,\mathrm{d}y\right]\mathrm{d}k', \end{aligned} \tag{4.27}$$

where we have used the behaviour of W^+ at infinity combined with the residue theorem to simplify the first term on the right-hand side.

The limiting behaviour of (3.4) gives $G(\xi) \sim b_0 \xi^{-1/2}$. Watson's lemma (Hinch 1991) then states that the Fourier transform $\hat{G}^-$ must behave as

$$\hat{G}^-(k) \sim b_0 \sqrt{2\pi}/[(\mathrm{i}+1)k^{1/2}] + o(k^{-1/2}) \tag{4.28}$$

for $k \to \infty$ in the lower half-plane. But

$$\hat{G}^-(k) = \Omega(k)/W^-(k) - f^-(k)/W^-(k). \tag{4.29}$$

Ω is entire and therefore either has polynomial behaviour or an essential singularity at infinity. With $W^-(k) \sim k^{-1/2}$, the only Ω that is consistent with $\hat{G}^-(k)$ remaining bounded is therefore $\Omega \equiv 0$.

To find b_0 in (4.28), we still need to identify the limiting behaviour of $f^-(k)/W^-(k)$ and hence of f^- at infinity. The only complication is the integral

$$h_2(k') := \int_0^1 \frac{\sinh\left[(k'^2 + \mathrm{i}k'V)^{1/2}(1-y)\right]}{\sinh\left[(k'^2 + \mathrm{i}k'V)^{1/2}\right]} \hat{b}(k', y)\,\mathrm{d}y, \tag{4.30}$$

which we cannot compute in closed form. The integral is clearly continuous in k'. At issue is only its behaviour for large k'. This is dominated by the singularity in $b(\xi, y)$ at the origin. We have $b(\xi, y) = 1/(\pi r) + \tilde{b}(\xi, y)$, where $r = \sqrt{\xi^2 + y^2}$ as before; $\tilde{b}$ is bounded and behaves as $\xi/(2r)$ near the origin, with $\tilde{b} - \xi/(2r)$ uniformly Lipschitz continuous throughout the domain, and smooth except at the origin.

A standard identity gives $\mathscr{F}(1/r) = 2\mathrm{K}_0(|k|y)$ (Abramowitz & Stegun 1972), where K_μ denotes the μth-order modified Bessel function of the second kind. For large k', we have

$$\begin{aligned}\int_0^1 \frac{\sinh\left[(k'^2 + \mathrm{i}k'V)^{1/2}(1-y)\right]}{\sinh\left[(k'^2 + \mathrm{i}k'V)^{1/2}\right]} \mathrm{K}_0(|k'|y)\,\mathrm{d}y &\sim \int_0^1 \exp(-|k'|y)\mathrm{K}_0(|k'|y)\,\mathrm{d}y \\ &= \frac{1}{|k'|}\int_0^{|k'|} \exp(-Y)\mathrm{K}_0(Y)\,\mathrm{d}Y \\ &\sim \frac{1}{|k'|},\end{aligned} \tag{4.31}$$

with $Y = |k'|y$. The error in this approximation is exponentially small in k'. It can further be shown that the contribution of $\tilde{b}$ to h_2 behaves as $O(k'^{-2})$. Hence $W^-(k')h_2(k')$ is integrable, with large-k' behaviour

$$|W^-(k')h_2(k')| \sim 2|k'|^{-3/2}/\pi + O(k'^{-5/2}) \quad \text{as } k' \to \pm\infty. \tag{4.32}$$

From (4.27), it then follows that at leading order in large k,

$$\begin{aligned}\frac{f^-(k)}{W^-(k)} \sim \Bigg(&\mathrm{i}(1-\nu)W^+(\mathrm{i}\epsilon) - \frac{\alpha}{2\pi i}\int_{-\infty}^{\infty} W^-(k') \\ &\times \left[\int_0^1 \frac{\sinh\left[(k'^2 + \mathrm{i}k'V)^{1/2}(1-y)\right]}{\sinh\left[(k'^2 + \mathrm{i}k'V)^{1/2}\right]} \hat{b}(k', y)\,\mathrm{d}y\right] \mathrm{d}k'\Bigg) \frac{1}{k^{1/2}}.\end{aligned} \tag{4.33}$$

In fact, it can be shown (by determining the contribution of $\tilde{b}$ to $h_2(k)$ up to $O(k^{-3})$, splitting the range of integration in (4.27) into a central region and semi-infinite tails, and restricting k to a wedge $\mathrm{Im}(k) < -\delta|\mathrm{Re}(k)|$) that the correction to (4.33) is of $O(k^{-3/2})$.

Comparing (4.33) with (4.28), we can identify $b_0(\mathrm{i}+1)\sqrt{\pi/2}$ with the coefficient of $k^{-1/2}$ (the term in round brackets) on the right-hand side of (4.33). From § 3, we require that heat flux at the origin be non-singular, so that $b_0 = 0$. The coefficient of $k^{-1/2}$ in (4.33) must therefore vanish. This constraint can be written in the form

$$\frac{1-\nu}{\alpha} = \frac{-1}{2\pi W^+(\mathrm{i}\epsilon)} \int_{-\infty}^{\infty} W^-(k') \left[\int_0^1 \frac{\sinh\left[(k'^2 + \mathrm{i}k'V)^{1/2}(1-y)\right]}{\sinh\left[(k'^2 + \mathrm{i}k'V)^{1/2}\right]} \hat{b}(k', y)\, \mathrm{d}y' \right] \mathrm{d}k'. \tag{4.34}$$

Recall that we eventually need to take the limit $\epsilon \to 0$; with this in mind can replace $W^+(\mathrm{i}\epsilon)$ by $W^+(0)$ above.

Equation (4.34) is then the relationship we seek, albeit in implicit form. Suppose we know the dimensional migration velocity V as well as the temperature difference $T_s - T_m$ and ice thickness H. Together, these give us the dimensionless migration velocity V^* that appears on the right-hand side of (4.34) (recall that we dropped the asterisks on non-dimensionalization). We can then compute the integrals on the right-hand side, and therefore find the corresponding value of $(1-\nu)/\alpha$. Given geothermal heat flux q_{geo} and the definition of α and ν in (4.1), this determines what the corresponding lateral shear stress τ_s must be. This calculation is however the reverse of what is likely to be needed in practice: instead of being given a migration velocity, we are more likely to know the lateral shear stress τ_s *a priori* from the force balance of the ice stream, as well as q_{geo}, $T_s - T_m$ and H. In that case, the corresponding migration rate V is defined implicitly by (4.34).

Once the constraint (4.34) is satisfied, it is straightforward to find the function $\hat{G}^-(k)$ and hence $\hat{F}^+(k)$, from which the Fourier transform $\hat{\Theta}_\epsilon$ of temperature can be reconstructed. This is not however our primary aim here; instead we are mostly interested in the relationship between velocity V and the proxy $\alpha/(1-\nu)$ for lateral shear stress. Before computing this, we have to address a complication: it is not immediately obvious that $(1-\nu)/\alpha$ calculated from (4.34) is necessarily real, as is required physically. We provide a proof in appendix C.

4.3. *Numerical method*

The right-hand side of (4.34) can be computed by relatively straightforward numerical quadratures, requiring some care with the infinite ranges of integration and Cauchy principal value integrals involved. We only sketch the details here.

Integration over the real axis is generally handled by splitting the range of integration into $(-\infty, k_1)$, (k_1, k_2) and (k_2, ∞), with $k_1 < 0 < k_2$ fixed. We change variables to $v = |k|^{-1/2}$ outside the finite interval (k_1, k_2) to transform the 'tails' $(-\infty, k_1)$ and (k_2, ∞) to a finite range of integration. Under this change of variables, an integrand behaving as $k^{-3/2}$ at large k yields a bounded integrand with respect to v. We subdivide the range of integration further to capture regions with significant variations in the integrand as necessary, and Gaussian quadratures are used to evaluate the resulting integrals. Multiple integrals are handled by a standard separation of variables (Isaacson & Keller 1966, § 7.3).

The sole exception to this procedure is the calculation of the Fourier transform of b. We use the cut-off function defined in (4.8) to define $b(x, y)$, and apply a fast Fourier transform to compute $\hat{b}$, splitting off the singular part of b first as indicated

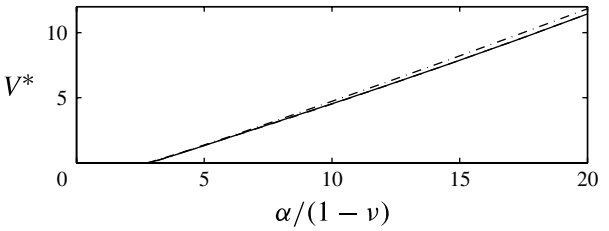

FIGURE 4. The migration velocity V^* as a function of the heating parameter $\alpha/(1-\nu)$ is shown as a solid black line. The dashed line (barely visible next to the solid line) shows a least-squares fit to a quadratic f_{20} over the range shown in the figure. The dot-dashed line shows a least-squares fit to a quadratic f_{120} over a larger range.

below equation (4.30); $\hat{b}(k,y)$ is then interpolated onto the Gaussian integration nodes for the remaining integrals. For large k, we use the asymptotic behaviour $\hat{b}(k,y) \sim 2\mathrm{K}_0(|k|y)/\pi - \mathrm{i}|k|yK_1(|k|y)/k$.

Boundary values of Cauchy integrals are required in evaluating $W_2^{\pm}(k)$ and $f^{\pm}(k)$. These are computed using Plemelj's formulae, dealing with principal value integrals as

$$PV\int_{-\infty}^{\infty}\frac{\phi(k')\,\mathrm{d}k'}{k'-k} = \int_{k-K}^{k+K}\frac{\phi(k')-\phi(k)}{k'-k}\,\mathrm{d}k' + \int_{-\infty}^{k-K}\frac{\phi(k')\,\mathrm{d}k'}{k'-k} + \int_{k+K}^{\infty}\frac{\phi(k')\,\mathrm{d}k'}{k'-k}, \quad (4.35)$$

where K is an arbitrary fixed positive number; the expressions on the right are then all ordinary integrals.

5. Results

For clarity, we re-introduce the asterisks on dimensionless variables here: recall that dimensional variables and their dimensionless counterparts are related simply by the scalings in § 4.1

The theoretical development in § 4 shows that the scaled migration velocity V^* is a function of the shear heating rate parameter $\alpha/(1-\nu)$ alone. All combinations of forcing parameters can be collapsed onto this single relationship. In a more comprehensible dimensional form, substituting from § 4.1, this relationship can be written as

$$V = \frac{\kappa}{\rho c H} f\left(\frac{\tau_s^2 H}{\eta\left[\kappa(T_m - T_s)/H - q_{geo}\right]}\right), \quad (5.1)$$

where V is the dimensional migration velocity and f is a function of a single argument. Figure 4 shows the shape of the function f as a solid black line, plotting $V^* = \rho c H V/\kappa = f(\alpha/(1-\nu))$ against $\alpha/(1-\nu) = \tau_s^2 H/\{\eta[\kappa(T_m - T_s)/H - q_{geo}]\}$.

The plot has two main features. Firstly, f is positive only when its argument exceeds a critical value. Physically, this means that a widening of the ice stream requires a minimum amount of shear heating. In figure 4 positive values of V^* correspond to $\alpha/(1-\nu) \geqslant 2.749$, or equally to

$$\tau_s^2 \geqslant \frac{2.749\eta[\kappa(T_m - T_s)/H - q_{geo}]}{H}. \quad (5.2)$$

This is physically realistic: in the absence of shear heating, the temperature field near the transition point is dominated by the cooling-fin effect described in § 3, and the temperate part of the bed is subject to intense heat loss that will cause the ice stream

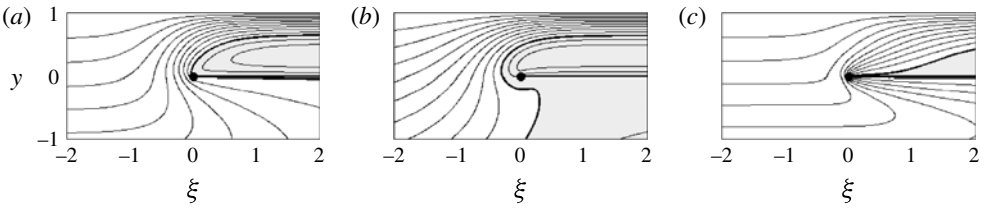

FIGURE 5. Controls on migration rate: the temperature field $T^*(\xi^*, y^*)$ around the transition point $(\xi^*, y^*) = (0, 0)$ (note that the figure labels omit asterisks for visual clarity) for a heating rate of $\alpha/(1-\nu) = 7.609$, but for different V^*. These are computed from the linear system (4.9) using (4.24) and (4.27), but not all have V constrained through (4.34). Contour intervals are 0.1 and temperate regions $T^* > 0$ are shown in grey, while $T = 0$ is a heavy black curve. The transition point is marked by a solid black dot, with the temperate bed shown as a solid line to the right; $\nu = 0.25$. (*a*) The temperature solution when the migration velocity is correctly related to migration rate through (4.34), which gives $V^* = 3$. Clearly there is a temperate zone above and to the right of the transition point. (*b*) The solution for $V^* = 0.3$. The migration velocity is now too slow, and the ice in the margins has longer to warm up. Consequently there is excessive build-up of heat, and the bed to the left of the transition point (where it should be frozen) is temperate. (*c*) The solution for $V^* = 15$; the temperate region is now shifted to the right and temperature contours are clustered around the origin, where there is a heat flux singularity that should cause the bed to freeze.

to narrow instead of widen. A finite amount of shear heating is required to overcome the cooling-fin effect, and this leads to the minimum value for τ_s above.

The second feature is that, for shear heating in excess of this minimum, the migration velocity is a monotonically increasing function of the shear heating rate. Again, this is realistic: larger heating rates will tend to cause temperatures near the transition point to rise. To prevent the temperature on the frozen side of the transition point from attaining the melting point, the margin has to migrate faster. This has the effect of allowing less time for the ice near the transition point to warm up, as the margin is constantly moving into colder ice outside the ice stream that has not yet been affected by the intense shear heating in the margin itself.

In fact, the function f can be fitted very well by low-order polynomials. Also shown in figure 4 as a dashed line (barely visible because it closely overlaps the solid line) is a least-squares fit to a quadratic over the range shown in the figure,

$$f_{20}\left(\frac{\alpha}{1-\nu}\right) = -1.645 + 0.579 \times \left(\frac{\alpha}{1-\nu}\right) + 0.00374 \times \left(\frac{\alpha}{1-\nu}\right)^2, \qquad (5.3)$$

which, over this range, has a maximum absolute error less than 0.045. In addition, the dot-dashed line shows a least-squares fit over the range $2.75 \leqslant \alpha/(1-\nu) \leqslant 120$:

$$f_{120}\left(\frac{\alpha}{1-\nu}\right) = -1.862 + 0.633 \times \left(\frac{\alpha}{1-\nu}\right) + 0.00258 \times \left(\frac{\alpha}{1-\nu}\right)^2. \qquad (5.4)$$

This diverges a little over the range shown in the figure, but maintains a maximum absolute error less than 0.5 for $\alpha/(1-\nu)$ up to 120.

We can also investigate the temperature field in the margin. Figure 5(*a*) shows the temperature field $T^*(\xi^*, y^*)$ around the transition point for $V^* = 3$, with the corresponding $\alpha/(1-\nu)$ given by (4.34). An obvious feature is the substantial region of ice with $T^* > 0$ (or $T > T_m$) extending above and to the right of the transition point at the origin. This is in line with our prediction in § 3, that widening of the ice stream

requires at least a small region of temperate ice near the transition point. As indicated before, we assume here that this simply corresponds to a zone of temperate ice; in reality, a temperate ice zone should be modelled separately based on the physics of melt drainage through a partially molten ice matrix (Fowler 2001), and its shape may not be exactly the same as that shown in figure 5. This will need to be addressed by future work.

The remaining panels in figure 5 also show solutions to (4.3) for the same value of $\alpha/(1-\nu)$ as in figure 5(*a*), but these solutions have arbitrarily chosen values of V^* that are not linked to $\alpha/(1-\nu)$ through (4.34). These solutions therefore violate either $T^*(\xi^*, 0) < 0$ for $\xi^* < 0$, or $T^*_{y^*}(\xi^*, 0)^+ - T^*_{y^*}(\xi^*, 0)^- \geqslant 0$ for $\xi^* > 0$. They are plotted to illustrate the physics that links migration rate to the shear heating rate, and are analogous to figure 2(*b*,*c*). Figure 5(*b*) shows the temperature field $T^*(\xi^*, y^*)$ with the migration rate reduced by a factor of 10 from figure 5(*a*). Here, the constraint that $T^* < 0$ at the bed to the left of the transition point is clearly violated, as the temperate ice zone extends down to the bed. The migration rate is too slow, allowing the build-up of excessive heat in the margin.

Figure 5(*c*) again uses the same heating rate $\alpha/(1-\nu)$, but with the migration rate increased by a factor of 5 from figure 5(*a*). In this case, migration into the colder ice to the left of the ice stream is so fast that shear heating is unable to warm the ice enough. The temperate ice zone has been shifted considerably away from the transition point, around which the ice remains cold. The temperature contours around the transition point also become closely spaced, indicating large heating fluxes out of the bed. This is in fact the result of the heat flux singularity predicted for the 'cooling fin' geometry of the temperate bed in § 3. Instantaneously, this temperature field would cause the water contained in the bed immediately to the right of the transition point to freeze; over time, the migration rate and temperature field should adjust to that shown in figure 5(*a*).

As a result, neither of the migration rates shown in figure 5(*b*,*c*) are viable. The solution in figure 5(*a*) in fact corresponds to the only migration rate for which there is neither melting to the left of the transition point, nor freezing to the right.

Figure 6 shows additional examples of physically acceptable temperature fields that do satisfy the conditions $T^*(\xi^*, 0) < 0$ for $\xi^* < 0$ and $T^*_{y^*}(\xi^*, 0)^+ - T^*_{y^*}(\xi^*, 0)^- \geqslant 0$ for $\xi^* > 0$ as required, so that V^* and $\alpha/(1-\nu)$ are linked through (4.34). Shown are solutions for different migration velocities, corresponding to different shear heating rates. The faster migration rates in figure 6(*b*) ($V* = 1$) and figure 6(*c*) ($V^* = 10$) correspond to more intense shear heating. Consequently the temperate ice zone above and to the right of the transition point becomes more extensive for larger V^*. However, they also correspond to less time available for heating, and this is evident in the isotherms below the bed, where no heat is generated. At higher migration velocities, these isotherms are flattened out, as less of the rock has been able to heat up.

6. Discussion

The main purpose of our theory is to allow models for ice-stream dynamics to include margin migration. A frequently used model for the flow of a wide and thin ice stream is the depth-integrated 'membrane stress' (or 'shallow shelf') approximation (MacAyeal 1989; Hulbe & MacAyeal 1999). Restricting ourselves to the same effectively two-dimensional geometry used above, so we consider variations in the cross-flow direction only, this can be reduced to (Raymond 1996)

$$\left(\tfrac{1}{2}BH|u_x|^{1/n-1}u_x\right)_x - \tau_b(u, N) - \rho g H \sin\beta = 0, \tag{6.1}$$

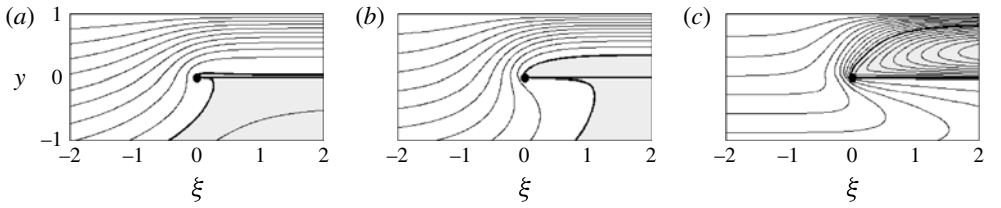

FIGURE 6. The temperature field $T^*(\xi^*, y^*)$ around the transition point $(\xi^*, y^*) = (0, 0)$; same line scheme as in figure 5, but all solutions now have V^* related to $\alpha/(1-\nu)$ through (4.34). Again, grey regions indicate $T^* > 0$, while the heavy black curve for $\xi^* > 0$, $Y^* = 0$ indicates $T^* = 0$ there. (*a*) $V^* = 0$, (*b*) $V^* = 1$ and (*c*) $V^* = 10$.

where H and u still denote ice thickness and velocity, and x is the cross-flow coordinate. The flow of ice is assumed to be a plug flow, with u dependent only on x; β is ice surface inclination in the along-flow direction, while ρ and g are density of ice and acceleration due to gravity, respectively. The basal shear stress τ_b may be an increasing function of velocity and of effective pressure at the bed (e.g. Budd, Keage & Blundy 1979; Fowler 1987), or independent of velocity and related to effective pressure through a Coulomb friction law as suggested by recent studies on Antarctic ice streams (Tulaczyk *et al.* 2000*a*; Schoof 2006). Effective pressure is defined as ice overburden pressure minus basal water pressure, and a complete model therefore requires coupling the ice flow model (6.1) to a description of water production, storage and transport. Recent work on ice-stream dynamics (Bougamont *et al.* 2011) has focused on this coupling to capture feedbacks between ice flow and water production (see also Fowler & Johnson 1996; Sayag & Tziperman 2008). However, existing models in general do not consider the thermal physics that occurs in the shear margins in order to determine their location, and frequently impose fixed margin locations (e.g. Hulbe & MacAyeal 1999).

In (6.1), the appropriate boundary condition at a margin $x = \pm x_m$ is $u(\pm x_m) = 0$ (Raymond 1996). For a given effective pressure N, this allows ice velocity to be computed straightforwardly as the solution of the elliptic problem (6.1). The shear margin model developed above is essentially a boundary layer model that must match in its far field with the bulk of the ice stream described by (6.1). The boundary layer model then furnishes a rate of margin migration in response to a shear stress imposed by the ice stream. Defining the lateral shear stress at the margin through

$$\tau_s = \tfrac{1}{2}B|u_x|^{1/n-1}\,u_x\big|_{x=x_m}, \tag{6.2}$$

the theory computes the rate of margin migration as in (5.1),

$$\dot{x}_m = V(\tau_s, q_{geo}, H, T_s - T_m). \tag{6.3}$$

Note that (5.1) strictly speaking only applies to Newtonian ice. A heuristic generalization to Glen's law can presumably be constructed by allowing viscosity in (5.1) to depend on stress as $\eta = (B/2)^n\,\tau_s^{1-n}$.

The theory as currently formulated may run into some difficulties, however, and these point to desirable improvements that future work will need to provide. The primary difficulty is that (6.3) is in fact a recipe for runaway widening of ice streams. Assuming a symmetric ice stream, the rate of widening is simply twice the migration rate V. The migration rate V as shown in figure 4 is a monotonically increasing function of lateral shear stress τ_s. For many Antarctic ice streams, velocities are limited by lateral shearing rather than by basal shear stress τ_b (e.g. Joughin *et al.*

2002). If we ignore τ_b as a result, then (6.1) predicts that lateral shear stress increases linearly with ice-stream width. Hence the rate of ice-stream widening is an increasing function of ice-stream width. This ought to lead to ever faster ice-stream widening in a positive feedback.

There is no evidence that this happens in nature, which leads us to look for a stabilizing mechanism. The migration rate V in (5.1) is not simply a function of lateral shear stress τ_s alone, but also an increasing function of ice thickness H. A reduction in H leads to less heat dissipation for the same lateral shear stress τ_s, and to faster conductive heat loss from the bed. A reduction in ice thickness H will therefore slow the widening of the ice stream. Hence, if the increased ice discharge associated with a wider ice stream leads to significant mass loss and hence a thinning of the ice stream, this may suppress runaway growth. Further research is needed to determine if this effect is sufficient.

An additional effect that is currently not included in our model is the advection of cold ice by ice flow across the shear margin (see also Echelmeyer *et al.* 1994; Jacobson & Raymond 1998). In reality, the parallel-slab geometry assumed in § 2 is misleading, as the ice surrounding most ice streams is thicker than the ice stream itself. This generates a surface slope that drives ice from these surrounding *ice ridges* across the shear margins and into the ice stream itself.

This form of advection plays much the same role in cooling the shear margin as migration does in our theory above. Rather than having to migrate outwards into colder ice to avoid excessive heating, the shear margin can now also be prevented from warming by that colder ice being actively advected across the shear margin (Echelmeyer *et al.* 1994; Jacobson & Raymond 1998). In fact, mathematically, the two effects enter in very similar ways: let $\boldsymbol{v}$ be the lateral inflow velocity in the (x, y)-plane. The obvious generalization of our model is to retain (2.2*c*)–(2.2*g*) and (2.4*b*), but to replace (2.4*a*) with

$$\rho c V T_\xi + \rho c \boldsymbol{v} \cdot \boldsymbol{\nabla} T - \kappa \nabla^2 T = \eta (u_\xi^2 + u_y^2) \tag{6.4}$$

with $\boldsymbol{\nabla} = (\partial/\partial\xi, \partial/\partial y)$, and $\boldsymbol{v}$ given by an appropriate model for the lateral inflow of ice across the shear margin.

This generalization cannot be solved using the Wiener–Hopf method in § 4 because the advection velocity $\boldsymbol{v}$ is not constant, and the Fourier transform of the advection term is not simply a multiple of the Fourier transform of temperature T; a more complicated direct numerical solution of the generalized model is required. Nonetheless, V and $\boldsymbol{v}$ obviously play similar roles in (6.4), and a crude approximation would be to suppose that the migration velocity V computed in § 5 is now the sum of the actual migration velocity and the vertically averaged x-component of $\boldsymbol{v}$. Denoting the latter quantity by $\bar{v}$, the actual margin migration velocity would then be

$$V = \frac{\kappa}{\rho c H} f\left(\frac{\tau_s^2 H}{\eta\left[\kappa(T_m - T_s)/H - q_{geo}\right]}\right) - \bar{v}, \tag{6.5}$$

so that the cross-margin flow slows down margin migration, as also predicted by Jacobson & Raymond (1998). Its stabilizing effect is ultimately also linked to lowering the ice surface in the ice stream: this has the effect of increasing the surface slope of the surrounding ice ridge, and therefore of driving faster ice flow across the margin at least temporarily, until ice gradient between ridge and stream is reduced as well.

Of course, (6.5) is purely an *ad hoc* fix. In reality, $\boldsymbol{v}$ is likely to exhibit a significant vertical shearing profile, and the strongest advective heat transport will happen closer to the surface. A likely consequence of this is to cool the surface

layers in the margin more than the ice near the bed, and thereby potentially to reduce the extent of temperate ice. A more sophisticated treatment of the temperate ice region is the second major improvement our model calls for; at present the complications introduced by producing a partial melt in the ice are completely ignored. Additionally, the effect of a non-constant viscosity, and in particular the coupling between dissipation, temperature and viscosity (Echelmeyer *et al.* 1994; Jacobson & Raymond 1998; Truffer & Echelmeyer 2003) will also need to be considered in future research. However, even with these improvements still to be made, our model still provides a useful test case for any numerical algorithm designed to solve a more complicated model for the margin, provided the additional physics can be 'switched off' in such a model.

There remains the need for observational verification, which we do not address in detail here. The change in basal conditions across shear margins is difficult to observe as direct access to the bed is usually not available. However, longer time series of shear margin migration combined with ice-stream velocity fields may eventually help to test the present models, as could any future drilling efforts; the latter are however likely to be difficult due to the often extensive crevasse fields at the surface of shear margins (Harrison *et al.* 1998).

7. Conclusions

We have developed a model for how the margin of an ice stream migrates outward over time. Our basic assumption is that a transition from slip to no slip occurs where the temperature of the bed drops below the melting point. That transition point can move in response to two competing effects. Intense shear heating in the margin will tend to warm the bed outside the area where slip is occurring, and therefore tend to widen the ice stream. The tip of the temperate bed region also has the geometry of a cooling fin, and is potentially subject to intense conductive heat loss that will tend to freeze the bed, causing the ice stream to narrow. The migration speed must balance these two effects. If the migration speed is too low, excess heat builds up and the bed warms, which leads to faster migration. If the migration speed is too large, the margin advances rapidly into colder ice with insufficient time for warming by shear heating. The cooling-fin effect then dominates, causing freezing of the bed, suppressing outward migration.

Our model shows how a steady migration speed can be computed by requiring that neither of these two scenarios occurs. Our results lead to two main conclusions. First, a widening of the ice stream invariably requires a region of temperate ice to form near the transition from temperate to cold bed. Such a temperate region was previously inferred by Perol (2011). Second, the widening rate is an increasing function of the lateral shear stress imposed on the margin. In addition, this lateral shear stress must exceed a critical minimum value below which no widening is possible; in fact, we expect the bed in the margins to freeze shut when this minimum value is not attained.

The model requires two improvements in future: a better treatment of the temperate ice zone, and the inclusion of advection of heat by ice flow across the margin. It is at present unclear if more sophisticated treatments of temperate ice will change our results qualitatively. The inclusion of lateral heat advection is likely to slow margin migration, depending on the advection speed.

Acknowledgements

This work was supported by a Canada Research Chair and NSERC Discovery Grant number 357193. I am grateful to M. Haseloff and I. Hewitt for discussions,

to the editor, M. G. Worster, and to R. Katz and two anonymous referees for their thorough reviews that have helped to improve this manuscript.

Appendix A. The near-field temperature solution

The validty of (3.4) can be demonstrated simply by substituting in (3.3). Here we show how to derive (3.4) as the general solution to the local heat flow problem (3.3) through a complex-variable method. Define the complex number $z = \xi + \mathrm{i}y$. Transforming to z and its conjugate $\bar{z} = \xi - \mathrm{i}y$ as independent variables, (3.3) can be re-written as (England 1971)

$$-4\frac{\partial^2 T}{\partial z \partial \bar{z}} = \begin{cases} \dfrac{\eta a_0^2}{k}(z\bar{z})^{-1/2} & \text{for } \mathrm{Im}(z) > 0, \\ 0 & \text{for } \mathrm{Im}(z) < 0. \end{cases} \tag{A 1}$$

This has a general solution

$$T(z,\bar{z}) = \begin{cases} -\dfrac{\eta a_0^2}{k}\left[(z\bar{z})^{1/2} + \dfrac{z}{2} + \dfrac{\bar{z}}{2}\right] + \phi(z) + \overline{\phi(z)} & \text{for } \mathrm{Im}(z) > 0, \\ \phi(z) + \overline{\phi(z)} & \text{for } \mathrm{Im}(z) < 0 \end{cases} \tag{A 2}$$

where $\phi(z)$ is analytic in the lower and upper half-planes, but not necessarily across the real axis. The boundary conditions in (3.3) state that

$$\phi(\xi)^+ + \overline{\phi(\xi)}^+ = \phi(\xi)^- + \overline{\phi(\xi)}^-, \tag{A 3a}$$

$$\mathrm{i}\left(\phi'(\xi)^+ - \overline{\phi'(\xi)}^+\right) = \mathrm{i}\left(\phi'(\xi)^- - \overline{\phi'(\xi)}^-\right) \quad \text{for } \xi < 0, \tag{A 3b}$$

$$\phi(\xi)^+ + \overline{\phi(\xi)}^+ = \frac{2a_0\xi}{k}, \quad \phi(\xi)^- + \overline{\phi(\xi)}^- = 0 \quad \text{for } \xi > 0. \tag{A 3c}$$

Differentiating (A 3*b*) with respect to ξ shows that ϕ' is analytic in the complex z-plane cut along the positive real axis, while similar differentiation of (A 3*c*) shows that $\mathrm{Re}(\phi'(\xi)^+) = \eta a_0^2/k$, $\mathrm{Re}(\phi'(\xi)^-) = 0$ for $\xi > 0$. Moreover, ϕ' is a complex temperature gradient, and must therefore be integrable along the real axis. Hence ϕ' is sectionally holomorphic in the sense of Muskhelishvili (1992). A straightforward reformulation as a pair of Hilbert problems results from defining $\Phi(z) = [\phi(z) + \overline{\phi(\bar{z})}]/2$, $\Psi(z) = [\phi(z) - \overline{\phi(\bar{z})}]/2$. Then Φ and Ψ are also sectionally holomorphic in the cut plane, satisfying $\Phi(\xi)^+ + \Phi(\xi)^- = 2a_0/k$, $\Psi(\xi)^+ - \Psi(\xi)^- = 2\eta a_0^2/k$. These have general solution

$$\Phi(z) = \frac{\eta a_0^2}{k} + z^{-1/2}P_1(z), \quad \Psi(z) = -\frac{a_0}{\pi \mathrm{i} k}\log(z) + P_2(z), \tag{A 4}$$

where $z^{-1/2}$ and $\log(z)$ have branch cuts along the positive real axis, taking their usual principal values as the branch cut is approached from above. Given the symmetry requirements imposed by the construction of Φ and Ψ, $P_1(z) = \sum_{n=0}^{\infty}\alpha_n z^n$ and $P_2(z) = \sum_{n=0}^{\infty}\beta_n z^n$ are convergent Taylor series with purely real and purely imaginary coefficients, respectively; the form of the coefficients can only be determined further if we apply additional far-field boundary conditions. The solution (3.4) can then be recovered if we recognize that $\phi'(z) = \Phi(z) + \Psi(z)$, and integrate subject to the boundary condition $\mathrm{Re}(\phi(\xi)^-) = 0$ for $\xi > 0$.

Appendix B. Behaviour near the transition point during freezing

A complete account of freezing near the tip of the temperate bed is beyond the scope of the present work and is given in a companion paper. This appendix focuses only on how a local heat flux singularity near the tip necessarily leads to inward migration of the transition point into the ice stream, and a narrowing ice stream.

We can dispense with the travelling wave form of (3.3) and revert to the original heat equation (2.2*a*)–(2.2*b*). Near the transition point, temperature is again dominated by diffusion, and the local heat flow model (3.3) continues to hold with $x - x_m(t) = r\cos(\theta)$, $y = r\sin(\theta)$. Hence we can assume a local solution for net heat flux out of the bed of the form given by (3.5). Suppose that there is a finite amount of water $h(x, t)$ stored per unit area the bed. If this evolves due to freezing, then

$$\rho_w L \frac{\partial h}{\partial t} = \kappa (T_\theta(r, 0) - T_\theta(r, 2\pi))/r, \tag{B 1}$$

where ρ_w is the density of water and L is latent heat of fusion. Using (3.5), this can be written as

$$\frac{\partial h}{\partial t} = -Ar^{-1/2} = -A\,(x - x_m(t))^{-1/2}, \tag{B 2}$$

where $A = -\kappa b_0/(\rho_w L) > 0$ during freezing. Let

$$h(x, 0) = h_0(x) \tag{B 3}$$

describe the initial fluid layer thickness, and pick the location of the origin such that $x_m(0) = 0$. Integrating (B 2) gives

$$h(x, t) = h_0(x) - \int_0^t \frac{A}{(x - x_m(t'))^{1/2}}\,\mathrm{d}t'. \tag{B 4}$$

To find how the transition point $x_m(t)$ moves, the trick is to recognize that h becomes zero at $x = x_m(t)$. Hence

$$0 = h_0(x_m(t)) - \int_0^t \frac{A}{(x_m(t) - x_m(t'))^{1/2}}\,\mathrm{d}t'. \tag{B 5}$$

This turns into Abel's integral equation for the rate of transition point migration if we treat x_m as the independent variable and t as a dependent variable. Let $\xi = x_m(t)$ and change variables in the integral to $x'_m = x_m(t')$ and reserve x_m to mean $x_m(t)$. Note that

$$\frac{\mathrm{d}t'}{\mathrm{d}\xi'} = 1 \Big/ \frac{\mathrm{d}x_m(t')}{\mathrm{d}t'} = 1/\dot{x}_m, \tag{B 6}$$

where we can treat the migration rate $\dot{x}_m = \mathrm{d}x_m(t')/\mathrm{d}t'$ as a function of x'_m. Equation (B 5) then becomes

$$h_0(\xi) = \int_0^\xi \frac{A}{(x_m - x'_m)^{1/2}} \frac{1}{\dot{x}_m(x'_m)}\,\mathrm{d}x'_m. \tag{B 7}$$

This has solution (e.g. Debnath & Mikusiński 1999)

$$\frac{1}{\dot{x}_m(x_m)} = \frac{1}{A\pi} \frac{\mathrm{d}}{\mathrm{d}x_m} \int_0^{x_m} \frac{h_0(x'_m)}{(x_m - x'_m)^{1/2}}\,\mathrm{d}x'_m. \tag{B 8}$$

Given the initial fluid thickness $h_0(\xi)$, this can be solved by separation of variables. Recalling that we have chosen $x_m(0) = 0$,

$$\int_0^{x_m(t)} \frac{h_0(x'_m)}{(x_m(t) - x'_m)^{1/2}}\,\mathrm{d}x'_m = A\pi t. \tag{B 9}$$

This defines $x_m(t)$ implicitly, and clearly $x_m(t) > 0$ for $t > 0$ provided the initial thickness h_0 is positive: the margin moves to the right, or into the ice stream. Further details are given in the companion paper (Schoof, 2012, submitted).

Appendix C. Real-valuedness of $(1-\nu)/\alpha$

We can demonstrate that the right-hand side of (4.34) is real by showing that it is unchanged under complex conjugation. This is somewhat laborious but ultimately simple.

Let an overbar denote complex conjugation. Taking care with the branches defined for the various square roots and logarithms in § 4, it can be shown that for real k,

$$\overline{(k^2 + \mathrm{i}kV)^{1/2}} = ((-k)^2 + \mathrm{i}(-k)V)^{1/2}, \tag{C 1a}$$

$$\overline{(k - \mathrm{i}V)^{1/2}} = \mathrm{i}\,((-k) - \mathrm{i}V)^{1/2}, \tag{C 1b}$$

$$\overline{k^{1/2}} = \mathrm{i}\,(-k)^{1/2}, \tag{C 1c}$$

and for k real or in the upper half-plane

$$\overline{(k + \mathrm{i}V)^{1/2}} = -\mathrm{i}\,(-\bar{k} + \mathrm{i}V)^{1/2}, \tag{C 2}$$

where the branches on the left- and right-hand sides are the same in each case. Then

$$\begin{aligned}\overline{\log(W_2(k))} &= \overline{\log\left(\frac{k^{1/2}\exp\left[(k^2+\mathrm{i}kV)^{1/2}\right]}{2\,(k-\mathrm{i}V)^{1/2}\sinh\left[(k^2+\mathrm{i}kV)^{1/2}\right]}\right)}\\ &= \log\left(\frac{\overline{k^{1/2}}}{\overline{(k-\mathrm{i}V)^{1/2}}}\frac{\exp\left[\overline{(k^2+\mathrm{i}kV)^{1/2}}\right]}{2\sinh\left[\overline{(k^2+\mathrm{i}kV)^{1/2}}\right]}\right)\\ &= \log(W_2(-k))\end{aligned} \tag{C 3}$$

and

$$\begin{aligned}\overline{W_2^{\pm}(k)} &= \exp\left(\frac{1}{-2\pi i}\int_{-\infty}^{\infty}\frac{\overline{\log(W_2(k'))}}{k'-\bar{k}}\,\mathrm{d}k'\right)\\ &= \exp\left(\frac{1}{2\pi i}\int_{-\infty}^{\infty}\frac{\log(W_2(k''))}{k''+\bar{k}}\,\mathrm{d}k''\right)\\ &= \overline{W_2^{\pm}(-\bar{k})},\end{aligned} \tag{C 4}$$

where $k'' = -k'$. On the real axis,

$$\begin{aligned}\overline{W^-(k)} &= \overline{W_2^-(k)}/\overline{(k-\mathrm{i}V)^{1/2}}\\ &= -\mathrm{i}W_2^-(-k)/\,((-k)-\mathrm{i}V)^{1/2}\\ &= -\mathrm{i}W^-(-k).\end{aligned} \tag{C 5}$$

Similarly, for k in the upper half-plane, $\overline{W^+(k)} = -\mathrm{i}W^+(-\bar{k})$, so $\overline{W^+(\mathrm{i}\epsilon)} = -\mathrm{i}W^+(\mathrm{i}\epsilon)$. Note also that the $b(\xi, y)$ is real, so that $\overline{\hat{b}(k, y)} = \hat{b}(-k, y)$. Then

$$\begin{aligned}
\overline{\left(\frac{1-\nu}{\alpha}\right)} &= \frac{1}{2\pi W^+(\mathrm{i}\epsilon)} \int_{-\infty}^{\infty} W^-(k') \left[\int_0^1 \frac{\sinh\left[(k'^2 + \mathrm{i}k'V)^{1/2}(1-y)\right]}{\sinh\left[(k'^2 + \mathrm{i}k'V)^{1/2}\right]} \hat{b}(k', y)\, \mathrm{d}y' \right] \mathrm{d}k' \\
&= \frac{1}{2\pi(-\mathrm{i})W^+(\mathrm{i}\epsilon)} \int_{-\infty}^{\infty} \overline{W^-(k')} \left[\int_0^1 \frac{\sinh\left[\overline{(k'^2 + \mathrm{i}k'V)^{1/2}}(1-y)\right]}{\sinh\left[(k'^2 + \mathrm{i}k'V)^{1/2}\right]} \overline{\hat{b}(k', y)}\, \mathrm{d}y' \right] \mathrm{d}k' \\
&= \frac{1}{2\pi(-\mathrm{i})W^+(\mathrm{i}\epsilon)} \int_{-\infty}^{\infty} (-i)W^-(k'') \left[\int_0^1 \frac{\sinh\left[(k''^2 + \mathrm{i}k''V)^{1/2}(1-y)\right]}{\sinh\left[(k''^2 + \mathrm{i}k''V)^{1/2}\right]} \hat{b}(k'', y)\, \mathrm{d}y' \right] \mathrm{d}k'' \\
&= \frac{1-\nu}{\alpha} \qquad \text{(C 6)}
\end{aligned}$$

as required, where $k'' = -k'$ as before.

REFERENCES

ABRAMOWITZ, M. & STEGUN, I. A. (Eds) 1972 *Handbook of Mathematical Functions*. Dover.

ALLEY, R. B. & BINDSCHADLER, R. A. (Eds) 2001 *The West Antarctic Ice Sheet: Behaviour and Environment*. American Geophysical Union.

ASCHWANDEN, A., BUELER, E., KHROULEV, C. & BLATTER, H. 2012 An enthalpy formulation for glaciers and ice sheets. *J. Glaciol.* **58** (209), 441–457.

BAMBER, J. L., VAUGHAN, D. G. & JOUGHIN, I. 2000 Widespread complex flow in the interior of the Antarctic ice sheet. *Science* **287** (5456), 1248–1250.

BARCILON, V. & MACAYEAL, D. R. 1993 Steady flow of a viscous ice stream across a no-slip/free-slip transition at the bed. *J. Glaciol.* **39** (131), 167–185.

BINDSCHADLER, R., VORNBERGER, P., BLANKENSHIP, D., SCAMBOS, T. & JACOBEL, R. 1996 Surface velocity and mass balance of Ice Streams D and E, West Antarctica. *J. Glaciol.* **42** (142).

BLANKENSHIP, D. D., BENTLEY, C. R., ROONEY, S. T. & ALLEY, R. B. 1987 Till beneath Ice Stream B. 1. Properties derived from seismic travel times. *J. Geophys. Res.* **92** (B9), 8903–8911.

BOUGAMONT, M., PRICE, S., CHRISTOFFERSEN, P. & PAYNE, A. J. 2011 Dynamic patterns of ice stream flow in a 3D higher-order ice sheet model with plastic bed and simplified hydrology. *J. Geophys. Res.* **116** (F04018) doi:10.1029/2011JF002025.

BUDD, W. F., KEAGE, P. L. & BLUNDY, N. A. 1979 Empirical studies of ice sliding. *J. Glaciol.* **23** (89), 157–170.

CARSLAW, H. S. & JAEGER, J. C. 1959 *Conduction of Heat in Solids*. Clarendon.

CUFFEY, K. M. & PATERSON, W. S. B. 2010 *The Physics of Glaciers*, 4th edn. Elsevier.

DEBNATH, L. & MIKUSIŃSKI, J. 1999 *Introduction to Hilbert Spaces with Applications*. Academic.

DÍAZ, J. I., MUÑOZ, A. I. & SCHIAVI, E. 2007 Existence of weak solutions to a system of nonlinear partial differential equations modelling ice streams. *Nonlin. Anal. Real World Appl.* **8**, 267–287.

ECHELMEYER, K. A., HARRISON, W. D., LARSEN, C. & MITCHELL, J. E. 1994 The role of margins in the dynamics of an active ice stream. *J. Glaciol.* **40** (136), 527–538.

ENGELHARDT, H. & KAMB, B. 1997 Basal hydraulic system of a West Antarctic ice stream: constraints from borehole observations. *J. Glaciol.* **43** (144), 207–230.

ENGLAND, A. H. 1971 *Complex Variable Methods in Elasticity*. J. Wiley & Sons.

FOWLER, A. C. 1987 Sliding with cavity formation. *J. Glaciol.* **33** (105), 255–267.

FOWLER, A. C. 2001 Modelling the flow of glaciers and ice sheets. In *Continuum Mechanics and Applications in Geophysics and the Environment* (ed. B. Straughan, R. Greve, H. Ehrentraut & Y. Wang), pp. 276–304. Springer.

FOWLER, A. C. & JOHNSON, C. 1996 Ice-sheet surging and ice-stream formation. *Ann. Glaciol.* **23**, 68–73.

HARRISON, W. D., ECHELMEYER, K. A. & LARSON, C. F. 1998 Measurement of temperature in a margin of Ice Stream B, Antarctica: implications for margin migration and lateral drag. *J. Glaciol.* **44** (148), 615–624.

HINCH, E. J. 1991 *Perturbation Methods*. Cambridge University Press.

HULBE, C. & FAHNESTOCK, M. 2007 Century-scale discharge stagnation and reactivation of the ross ice streams, west antarctica. *J. Geophys. Res.* **112** (F3), F0327.

HULBE, C. & MACAYEAL, D. R. 1999 A new thermodynamical numerical model of coupled ice sheet, ice stream, and ice shelf flow. *J. Geophys. Res.* **104** (B11), 25349–25366.

HUTTER, K. & OLUNLOYO, V. O. S. 1980 On the distribution of stress and velocity in an ice strip, which is partly sliding over and partly adhering to its bed, by using a Newtonian viscous approximation. *Proc. R. Soc. Lond.* A. **373**, 385–403.

HUTTER, K., YAKOWITZ, S. & SZIDAROWSKY, F. 1986 A numerical study of plane ice-sheet flow. *J. Glaciol.* **32** (111), 139–160.

ISAACSON, E. & KELLER, H. B. 1966 *Analysis of Numerical Methods*. J.Wiley & Sons.

IVERSON, N. R., HOOYER, T. S. & BAKER, R. W. 1998 Ring-shear studies of till deformation: Coulomb-plastic behaviour and distributed shear in glacier beds. *J. Glaciol.* **44** (148), 634–642.

JACOBEL, R., SCAMBOS, T. A., RAYMOND, C. F. & GADES, A. M. 1996 Changes in the configuration of ice stream flow from the West Antarctic ice sheet. *J. Geophys. Res.* **101**, 5499–5504.

JACOBSON, H. P. & RAYMOND, C. F. 1998 Thermal effects on the location of ice stream margins. *J. Geophys. Res.* **103** (B6), 12111–12122.

JOUGHIN, I., TULACZYK, S., BINDSCHADLER, R. & PRICE, S. F. 2002 Changes in west antarctic ice stream velocities: observation and analysis. *J. Geophys. Res.* **107** (B11), 2289.

KAMB, B. 1991 Rheological nonlinearity and flow instability in the deforming bed mechanism of ice stream motion. *J. Geophys. Res.* **96** (B10), 16585–16595.

MACAYEAL, D. R. 1989 Large-scale flow over a viscous basal sediment: theory and application to Ice Stream E, Antarctica. *J. Geophys. Res.* **94** (B4), 4017–4087.

MUSKHELISHVILI, N. I. 1992 *Singular Integral Equations*. Dover, (unabridged republication of 2nd Edn published by P. Noordhoff, Groningen, 1953).

NOBLE, B. 1958 *Methods Based on the Wiener–Hopf Technique for the Solution of Partial Differential Equations*. Pergamon.

PEROL, T. 2011 Why do west antarctica ice streams exist? Master's thesis, École Normale Supérieure de Paris, Paris, France.

RAYMOND, C. 1996 Shear margins in glaciers and ice sheets. *J. Glaciol.* **42** (140), 90–102.

SAYAG, R. & TZIPERMAN, E. 2008 Spontaneous generation of pure ice streams via flow instability: role of longitudinal shear stresses and subglacial till. *J. Geophys. Res.* **113**, B05411.

SCHOOF, C. 2004 On the mechanics of ice stream shear margins. *J. Glaciol.* **50** (169), 208–218.

SCHOOF, C. 2006 A variational approach to ice-stream flow. *J. Fluid Mech.* **556**, 227–251.

SIEGERT, M. J., WELCH, B., VIELI, A., BLANKENSHIP, D. D., JOUGHIN, I., KING, E. C., VIELI, G. J. M. C. L., PAYNE, A. J. & JACOBEL, R. 2004 Ice flow direction change in interior west antarctica. *Science* **305** (5692), 1948–1951.

TRUFFER, M. & ECHELMEYER, K. A. 2003 Of isbrae and ice streams. *Ann. Glaciol.* **36**, 66–72.

TULACZYK, S., KAMB, W. B. & ENGELHARDT, H. F. 2000*a* Basal mechanisms of ice stream b, west antarctica: 1. Till mechanics. *J. Geophys. Res.* **105** (B1), 463–481.

TULACZYK, S., KAMB, W. B. & ENGELHARDT, H. F. 2000*b* Basal mechanisms of Ice Stream B, West Antarctica: 2. Undrained plastic bed model. *J. Geophys. Res.* **105** (B1), 483–494.

VAN DER VEEN, C. J. & WHILLANS, I. M. 1996 Model experiments on the evolution and stability of ice streams. *Ann. Glaciol.* **23**, 129–137.